

A Pair of Early- and Late-Forming Galaxy Cluster Samples: Evidence of Halo Assembly Bias?

YEN-TING LIN,¹ HIRONAO MIYATAKE,^{2,3} HONG GUO,⁴ HUIYUAN WANG,⁵ KAI-FENG CHEN,^{6,1} TING-WEN LAN,^{7,8}
YU-YEN CHANG,⁹ XIAOHU YANG,¹⁰ AND HOJUN MO¹¹

¹*Institute of Astronomy and Astrophysics, Academia Sinica (ASIAA), Taipei 10617, Taiwan*

²*Kobayashi-Maskawa Institute for the Origin of Particles and the Universe (KMI), Nagoya University, Nagoya, 464-8602, Japan*

³*Kavli Institute for the Physics and Mathematics of the Universe (WPI), The University of Tokyo Institutes for Advanced Study (UTIAS), The University of Tokyo, Chiba 277-8583, Japan*

⁴*Shanghai Astronomical Observatory, Shanghai 200030, China*

⁵*Key Laboratory for Research in Galaxies and Cosmology, Department of Astronomy, University of Science and Technology of China, Hefei, Anhui 230026, China*

⁶*Department of Physics, Massachusetts Institute of Technology, Cambridge, MA 02139, USA*

⁷*Department of Physics, National Taiwan University, Taipei 10617, Taiwan*

⁸*Graduate Institute of Astrophysics, National Taiwan University Taipei 10617, Taiwan*

⁹*Department of Physics, National Chung Hsing University, Taichung 402, Taiwan*

¹⁰*Department of Astronomy, Shanghai Jiao Tong University, Shanghai 200240, China*

¹¹*Department of Astronomy, University of Massachusetts, Amherst, MA 01003, USA*

Submitted to ApJL

ABSTRACT

The halo assembly bias, a phenomenon referring to dependencies of the large-scale bias of a dark matter halo other than its mass, is a fundamental property of our standard cosmological model. First discovered in 2005 via high-resolution numerical simulations, it has been proven very difficult to be detected observationally, with only a few convincing claims of detection thus far. The main obstacle lies in finding an accurate proxy of the halo formation time. In this study, by utilizing a constrained simulation that can faithfully reproduce the observed structures larger than ~ 2 Mpc in the local universe, for a sample of about 630 massive clusters at $z \leq 0.12$, we find their counterpart halos in the simulation and use the mass growth history of the matched halos to estimate the formation time of the observed clusters. This allows us to construct a pair of early- and late-forming clusters, with similar mass as measured via weak gravitational lensing, and large-scale bias differing at at least 4σ level, implying a detection of assembly bias.

Keywords: Large-scale structure of the universe — Galaxy clusters — Observational cosmology

1. INTRODUCTION

It has been well-known for more than a decade that, although the large-scale bias of dark matter halos is primarily a function of halo mass, it also has secondary dependencies on other halo properties such as the formation time, concentration, spin, etc (e.g., Gao et al. 2005; Jing et al. 2007). Such dependencies are loosely referred to as assembly bias (AB; see e.g., Mao et al. 2018; Wechsler & Tinker 2018). As AB is a subtle, yet solid feature of the cold dark matter model with a cosmological constant (Λ CDM), a solid observational

detection of the phenomenon will serve as a critical validation of the model.

In this study, we restrict ourselves to investigating the AB as manifested by the differences in halo formation time; that is, we aim to detect differences in the large-scale bias for halos of the same mass but with different formation times. Numerous studies have shown that the amplitude of halo AB is dependent on the halo mass (and to some degree, the definition of halo formation time and even the definition of a halo itself; see Mansfield & Kravtsov 2020 for details). In general it is more prominent for low mass halos, while less so at the massive end such as galaxy clusters. In our earlier attempt to detect AB in halos of mass comparable to that of the Milky Way ($\sim 10^{12} M_{\odot}$), we did not find convincing evidence for AB (Lin et al. 2016). It is likely due to our proxy for halo for-

mation time, namely the mean stellar age of central galaxies derived from spectra provided by the Sloan Digital Sky Survey (SDSS; York et al. 2000), is not of sufficient accuracy.

Using a large sample of SDSS redMaPPer clusters (Rykoff et al. 2014), Miyatake et al. (2016, hereafter M16) claimed a strong detection of AB, which unfortunately turned out to be mainly due to the projection effect; briefly speaking, the formation time proxy used by M16, namely the spatial concentration of photometrically selected potential cluster member galaxies, is contaminated by large-scale correlated structures along the line-of-sight, which mimics the AB signal (Zu et al. 2017; Sunayama & More 2019).

It is thus clear that, in the pursuit of detection of the AB signal, one of the main challenges is to have a robust proxy of halo formation time (while ensuring similar halo masses between early- and late-forming samples being another challenging aspect).

Here we present a novel approach to the estimation of halo formation time, which makes heavy use of the forward-modeling-based numerical simulation *Elucid* (Wang et al. 2016). *Elucid* is designed to reproduce the structures larger than ~ 2 Mpc as observed by the SDSS galaxy sample (Strauss et al. 2002) out to a redshift $z = 0.12$. As such, by matching a galaxy cluster sample drawn from the cluster and group catalog of Yang et al. (2007, hereafter Y07), we can find a one-to-one correspondence between the observed clusters and the simulated halos, whereby the cluster formation time is derived from the halo mass growth history (MGH). This method then allows us to split the cluster sample into early- and late-forming subsamples; based on mass measurements from weak gravitational lensing (WL) and large-scale bias derived from cluster-galaxy cross correlation, we show that a pair of early- and late-forming cluster samples exhibits the signature of AB at $> 5\sigma$ level, making this study among the first of a robust detection of AB at cluster mass scales ($\sim 10^{14} M_{\odot}$; see also Zu et al. 2021).

This Letter is structured as follows: in Section 2 we describe the key elements of our analysis. We construct a pair of early- and late-forming cluster samples that exhibits the AB signal, and examine the properties of cluster galaxy population of the samples in Section 3. We discuss the implications and prospects of our methods in Section 4.

Throughout this Letter we adopt a *WMAP5* (Komatsu et al. 2009) Λ CDM model, where $\Omega_m = 0.258$, $\Omega_{\Lambda} = 0.742$, $H_0 = 100h$ km s $^{-1}$ Mpc $^{-1}$ with $h = 0.71$, $\sigma_8 = 0.8$, which is employed by *Elucid* (Wang et al. 2014, 2016). All optical magnitudes are in the AB photometry system (Oke & Gunn 1983, please do not to be confused with assembly bias).

2. METHODOLOGY

Here we provide an overview of the main elements of our analysis. The basis of this work, the constrained simulation

Elucid, is presented in Section 2.1. Our cluster sample, and the way we match it to the simulated halos from *Elucid*, are described in Section 2.2. We then turn to our key observables, clustering and WL measurements, in Sections 2.3 and 2.4.

2.1. Constrained Simulation *Elucid*

The methodology behind *Elucid* can be found in Wang et al. (2014). Basically, a nonlinear density field is provided to a Hamiltonian Markov Chain Monte Carlo (HMC) algorithm combined with particle-mesh (PM) dynamics, which is able to reconstruct the initial linear density field. That density field is then evolved to the present-day with high resolution N -body simulations.

For the specific simulation used in this work, the nonlinear density field is constructed based on the group catalog of Y07, which itself is based on SDSS data release 7 (DR7; Abazajian et al. 2009). Given that the galactic systems in the Y07 catalog are complete down to a mass limit of $\approx 10^{12} h^{-1} M_{\odot}$ at $z \sim 0.12$, the nonlinear density field is estimated using only halos above that mass limit and in the redshift range 0.01 – 0.12, lying within the northern Galactic cap region of the DR7 footprint. The reconstructed initial density field is then evolved with 3072^3 particles in a $500h^{-1}$ Mpc box, using a modified version of GADGET-2 (Springel et al. 2005; Wang et al. 2016). Tests based on detailed mock galaxy samples showed that the typical scatter between the true (nonlinear) density field and the reconstructed one is 0.23 dex when smoothed over a scale of $2h^{-1}$ Mpc (Wang et al. 2016), which is about the typical size of a massive cluster, and is thus a good match for our purpose.

2.2. Galaxy Cluster Sample Selection

To match real clusters to the simulated halos in *Elucid*, we use the model C version of the Y07 catalog. As shown in Wang et al. (2016), only part of the SDSS DR7 footprint is covered in the reconstructed volume, and we end up with 644 clusters with mass $M_{200m} \geq 10^{14} h^{-1} M_{\odot}$. Here the mass is defined within a radius r_{200m} , within which the mean density is 200 times the mean density of the universe at the redshift of the cluster. The matching between the Y07 clusters and the *Elucid* halos is done in the following fashion: for a given cluster with mass M_1 , we search all simulated halos with a distance to the position of the cluster in the simulation less than $4h^{-1}$ Mpc. We have properly taken into account the redshift space distortion effect of clusters, by moving dark matter halos to redshift space using their peculiar velocities along the line of sight. Let us denote the mass of halos that lie within the sphere as M_2 . For all halos with mass satisfying $|\log(M_1/M_2)| < 0.5$, we select the one with the smallest $|\log(M_1/M_2)|$ as the matched halo. If no halo satisfies the

above condition, then the cluster is discarded from the sample. Out of 644 clusters, we find 634 matches this way.

For the clusters with a counterpart halo, we extract the MGH of the main subhalo (that is, simply following the main trunk of the merger tree), and derive several formation time indicators, such as z_{80} , z_{50} , z_{20} , and z_{mah} . While the first three correspond to the redshifts when a halo first reaches 80%, 50% and 20% of its final ($z = 0$) mass, the last quantity is obtained by first fitting the MGH by the form

$$M(z) \propto \exp(-\alpha z), \quad (1)$$

and then setting $z_{\text{mah}} \equiv 2/\alpha - 1$ (Wechsler et al. 2006).

2.3. Cluster-Galaxy Cross Correlation Function

With only ~ 600 clusters, inferring the large-scale bias b via auto-correlation function is challenging. We naturally opt for cluster-galaxy cross correlation $w_{p,gc}$ (a method also used by Medezinski et al. 2019): by comparing the $w_{p,gc}$ of early- and late-forming clusters at scales $10 - 30h^{-1}$ Mpc, we can then infer the relative bias of the two populations of clusters.

Following Guo et al. (2017), we measure the cross-correlation function $w_p(r_p)$ between our cluster samples and a volume-limited galaxy sample drawn from SDSS DR7 main spectroscopic sample with the r -band absolute magnitude $M_r \leq -20.5$ and $0.02 \leq z \leq 0.132$. The $w_p(r_p)$ measurement are calculated using the Landy & Szalay (1993) estimator, with r_p being the projected separation of the galaxy pairs. We choose logarithmic r_p bins with a width $\Delta \log r_p = 0.2$ from 0.1 to $63.1h^{-1}$ Mpc. The maximum line-of-sight integration length π_{max} is set to $40h^{-1}$ Mpc. Setting π_{max} to larger values does not change our results. The uncertainties in the w_p measurements are obtained by running 400 jackknife resampling.

2.4. Weak Gravitational Lensing Measurements

We measure weak gravitational lensing signals as the average excess surface mass density $\Delta\Sigma$ by stacking ~ 600 clusters in the same manner as M16, which followed the procedure described in Mandelbaum et al. (2013). We use the shape catalog based on the photometric galaxy catalog from SDSS DR8 (Reyes et al. 2012). The shapes of source galaxies were measured by the re-Gaussianization technique (Hirata & Seljak 2003). Systematic uncertainties in the shape measurements were investigated as done in Mandelbaum et al. (2005) and calibrations were performed using image simulations from Mandelbaum et al. (2012). Their photometric redshifts (photo- z) are estimated using the publicly available code ZEBRA (Feldmann et al. 2006; Nakajima et al. 2012). We choose logarithmic bins r_p with a width $\Delta r_p = 0.14$ from 0.025 to $50h^{-1}$ Mpc. We apply the photo- z correction, boost factor correction, and random signal correction following Mandelbaum et al. (2005)

and Nakajima et al. (2012). We estimate the covariance matrix using the jackknife technique as described in M16.

To infer the cluster mass, we fit a halo model that is similar to what is described in M16. We fit the signal within the range of $0.3 < r_p/[h^{-1}\text{Mpc}] < 3$, since this scale is not affected by 2-halo term. We use a truncated Navarro et al. (1997, hereafter NFW) profile, described in Takada & Jain (2003a,b), and assume that there are some fraction of off-centered clusters with respect to their true center. There are four fitting parameters in total: cluster mass M_{200m} , concentration parameter c_{200m} , fraction of centered clusters q_{cen} , and typical off-centering scale with respect to r_{200m} . For the q_{cen} , we employ a Gaussian prior $\mathcal{N}(0.8, 0.1)$. The cluster mass constraints are insensitive to the choice of the prior; when adopting a prior $\mathcal{N}(0.8, 0.2)$, the change in cluster mass is typical only a few percent.

3. RESULTS

3.1. Cluster Selection using z_{50} and z_{mah}

We start by splitting the clusters by either z_{50} or z_{mah} , using $z_{50,\text{div}} = 0.521$ and $z_{\text{mah},\text{div}} = 0.469$ for separating early- and late-forming clusters; the division redshifts are chosen to make the numbers of clusters in the two samples as close as possible. The mean masses of the resulting z_{50} -selected 323 early-forming and 311 late-forming clusters are $M_{200m} = (1.54 \pm 0.22) \times 10^{14}h^{-1} M_{\odot}$ and $(1.51 \pm 0.22) \times 10^{14}h^{-1} M_{\odot}$, respectively. In Figure 1 (upper panels), we show the lensing signals on the left side, while the projected cluster-galaxy correlation function on the upper right panel. The lower right panel shows the ratio of $w_{p,\text{early}}/w_{p,\text{late}} = b_{\text{early}}/b_{\text{late}}$. To quantify the difference between the $w_{p,\text{early}}$ and $w_{p,\text{late}}$ measurements (in terms of their ratio), we follow the methodology developed in Lin et al. (2016, see Section 4.1.2 therein) and calculate

$$\chi^2 = \sum_{ij} (w_e(r_i)/w_l(r_i) - \xi) C_{ij}^{-1} (w_e(r_j)/w_l(r_j) - \xi), \quad (2)$$

where w_e and w_l are shorthands for $w_{p,\text{early}}$ and $w_{p,\text{late}}$, respectively, C is the covariance matrix built from the ratio between $w_{p,\text{early}}$ and $w_{p,\text{late}}$ and their associated jackknife samples, and constant $\xi = 1$. The errorbars of the w_p ratio shown in Figure 1 (as well as in Figures 2 and 3) are calculated based on the diagonal terms of the covariance matrix C . With $\chi^2 = 9.3$ from 3 degrees of freedom, over the scales from $12.9h^{-1}$ Mpc to $32.5h^{-1}$ Mpc (hereafter the ‘‘mid-range’’), we find that the two samples have a probability $p = 0.0258$ to be drawn from the same parent population (i.e., having the same large-scale bias). Using the full scale as shown in the Figure ($8.2h^{-1}$ Mpc to $51.5h^{-1}$ Mpc), the probability changes to $p = 0.0393$.

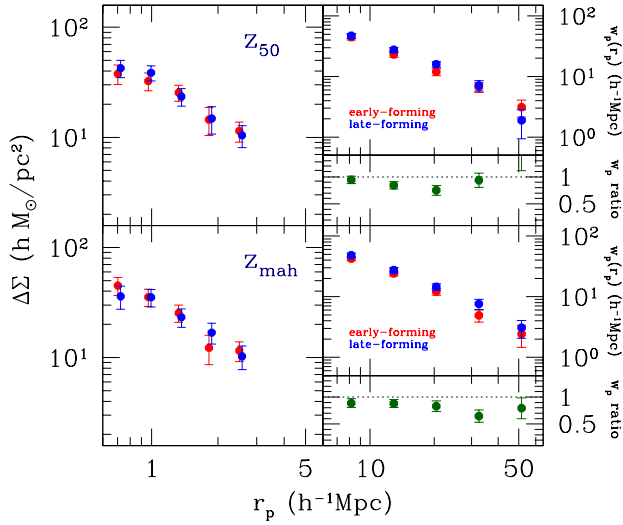


Figure 1. Weak lensing (left) and clustering (right) measurements as a function of projected distance for clusters split in half by z_{50} (upper panels) and z_{mah} (lower panels). The red and blue symbols represent early- and late-forming clusters, respectively. There are 323 and 311 early- and late-forming clusters when split by $z_{50, \text{div}} = 0.521$, while 316 and 318 clusters when split by $z_{\text{mah}, \text{div}} = 0.469$. WL masses for these samples are all very close, about $1.5 \times 10^{14} h^{-1} M_{\odot}$. The green points in the lower right panel are the ratio of the early-to-late w_p measurements, which is equivalent to the large-scale bias ratio $b_{\text{early}}/b_{\text{late}}$. The probability for these samples to be drawn from the same parent sample is $p = 0.0258$ (for the z_{50} -selected samples) and $p = 0.0295$ (for the z_{mah} -selected ones).

A similar result using cluster samples defined by z_{mah} is shown in the lower panels of Figure 1. The mean masses of 316 early-forming and 318 late-forming clusters are $M_{200m} = (1.52 \pm 0.23) \times 10^{14} h^{-1} M_{\odot}$ and $(1.46 \pm 0.21) \times 10^{14} h^{-1} M_{\odot}$, respectively. Using Eqn. 2, we find that the two samples have a probability $p = 0.0295$ (0.0152) to be consistent using the measurements from the mid-range (full-scale).

We then further seek stronger signals by exploring the extremal of the age distribution. However, as pointed out by Chue et al. (2018), at the mass scale of our clusters (i.e., around $10^{14} h^{-1} M_{\odot}$), z_{50} may not be the best age indicator. Quantities such as z_{20} or z_{80} may better reflect the formation history.

3.2. Age Extremum Selection of Clusters

After testing with various age indicators mentioned above, it is found that, by selecting 138 oldest clusters with $z_{20} > 1.35$, paired with 121 youngest clusters with $z_{20} < 0.85$, both limited in the redshift range $z = 0.06 - 0.12$ and mass

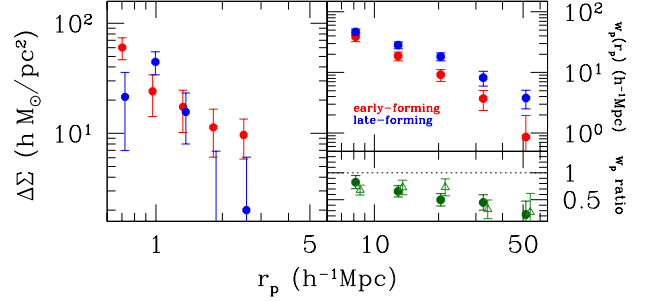


Figure 2. The $z_{20\text{ex}, Mz}$ set is selected to lie within the parameter space $\log M_{200m}/(h^{-1} M_{\odot}) = 14 - 14.5$ and $z = 0.06 - 0.12$. It consists of 138 oldest (with $z_{20} > 1.35$; red points) and 121 youngest (with $z_{20} < 0.85$; blue points), with masses within 1σ of each other; the probability for the two cluster samples to have the same large-scale bias is $p = 1.03 \times 10^{-10}$ using the clustering measurements in the mid-range. The open triangles in the lower right panel shows the relative bias of early- and late-forming halos (defined in the same way as the $z_{20\text{ex}, Mz}$ set) drawn from *Elucid* with identical halo mass range (and very similar mean masses). There is a good agreement in the relative biases between the simulation and our observation.

range $\log M_{200m}/(h^{-1} M_{\odot}) = 14 - 14.5$ (as estimated by Y07), we may have found a signal of AB. The mean masses are measured to be $M_{200m, \text{early}} = 1.26^{+0.35}_{-0.29} \times 10^{14} h^{-1} M_{\odot}$ and $M_{200m, \text{late}} = 0.95^{+0.26}_{-0.22} \times 10^{14} h^{-1} M_{\odot}$, consistent within 1σ (Figure 2). While the dividing redshifts are chosen so that we have at least 120 clusters in each sample, the redshift and halo mass ranges are selected to facilitate consistent cluster mass estimates. We shall refer to this pair of cluster samples as the $z_{20\text{ex}, Mz}$ set. Given the mass difference between the early- and late-forming clusters, we should compare the measured $b_{\text{early}}/b_{\text{late}}$ to the theoretically expected bias ratio $r_{b, \text{th}} = 1.11$ (assuming no effects from AB, as obtained by the bias-halo mass relation of Tinker et al. 2010), in order to evaluate the probability that the two samples have the same large-scale bias. We thus set $\xi = r_{b, \text{th}}$ in Eqn. 2, and find the probabilities to be $p = 1.02 \times 10^{-10}$ and 1.16×10^{-11} using the data from the mid-range and full scale, respectively.

Using the cluster-galaxy cross-correlation method described in Lan et al. (2016), we also measure the stacked galaxy surface density profiles of the early- and late-forming clusters in the $z_{20\text{ex}, Mz}$ set. Fitting the density profiles of galaxies with r -band absolute magnitudes of $-24 \leq M_r \leq -18$ with an NFW model, we find $c_{\text{early}} = 8.1^{+1.6}_{-1.3}$ and $c_{\text{late}} = 5.7^{+0.9}_{-0.8}$, which are consistent with the expectation that early-forming clusters would have a more spatially concentrated galaxy population, a premise of the analysis of M16. Within $r_{200m} \approx 1.5$ Mpc, about 80% of galaxies are red for both cluster samples.

We further examine the formation time of the cluster galaxy properties, particularly the brightest cluster galaxies (BCGs), using results from the full spectral fitting code STARLIGHT (Cid Fernandes et al. 2013) as well as the spectral energy distribution fitting technique presented in Chang et al. (2015). We do not find any appreciable differences in the ages of member galaxies in the early- and late-forming clusters.

Finally we investigate the magnitude gap Δ_{12} of the $z_{20\text{ex},\text{Mz}}$ set, which is the differences in the r -band absolute magnitudes between the BCG and the second most luminous galaxies (Tremaine & Richstone 1977). Using the cluster member catalog of Y07, we find that the median $\Delta_{12} = 0.44 \pm 0.05$ for the early-forming clusters, while that of the late-forming clusters is $\Delta_{12} = 0.38 \pm 0.05$. Although not providing strong constraints, this result is again consistent with the expectation that the gap increases as a cluster ages, as more and more massive/luminous satellites are cannibalized by the BCG via dynamical friction (Ostriker & Tremaine 1975).

3.3. Robustness of Detection

Given the relatively large uncertainties in the WL mass measurements of the $z_{20\text{ex},\text{Mz}}$ set, we first test their effect on the significance of our detection, by considering an extreme case where the differences in the large-scale clustering are primarily due to the cluster mass difference. To do so, we set $\xi = r_{\text{b,th}}$ to 0.92, the value corresponding to the bias ratio of halos of masses $M_{200\text{m,early,min}} = 0.97 \times 10^{14} h^{-1} M_{\odot}$ (i.e., 1σ lower than the mean mass of the early-forming clusters) and $M_{200\text{m,late,max}} = 1.21 \times 10^{14} h^{-1} M_{\odot}$ (1σ higher than the mean mass of the late-forming clusters) in Eqn. 2. The probability for such a case to occur is about 2.6%. Using the mid-range (full scale) clustering measurements, we find that the probability for the pair of cluster samples to have the same bias becomes $p = 7.49 \times 10^{-5}$ (5.40×10^{-5}). These correspond to a 4σ detection.

In the lower right panel of Figure 2, we further show the theoretically expected $b_{\text{early}}/b_{\text{late}}$ ratio as the open triangles, as derived from *Elucid*, in which the effect of AB *must* be present. We first select dark matter halos with masses $M_{200\text{m}} = (0.7 - 1.9) \times 10^{14} h^{-1} M_{\odot}$, then separate them into early- and late-forming using the same redshift division as done for the $z_{20\text{ex},\text{Mz}}$ set. We then cross-correlate the resulting 98 early-forming and 82 late-forming halos, which have mean masses of $(1.24 \pm 0.31) \times 10^{14} h^{-1} M_{\odot}$ and $(1.26 \pm 0.36) \times 10^{14} h^{-1} M_{\odot}$, respectively, with low mass halos in the mass range $\log M_{200\text{m}}/(h^{-1} M_{\odot}) = 11.5 - 12.5$, and derive the ratio between $w_{p,\text{early}}$ and $w_{p,\text{late}}$. The triangles appear to be consistent with our measurements (the solid points), indicating that the measured AB signal from the $z_{20\text{ex},\text{Mz}}$ set is similar in amplitude to that expected in

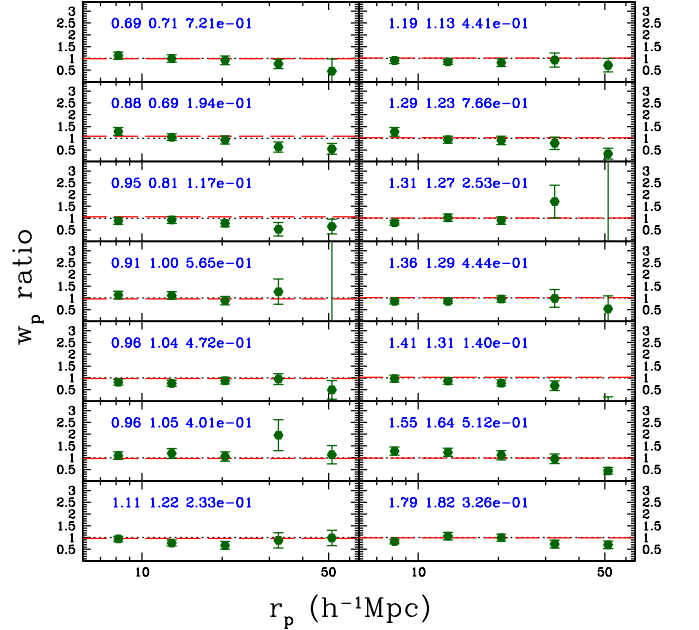


Figure 3. Ratio of $w_{p,\text{early}}/w_{p,\text{late}} = b_{\text{early}}/b_{\text{late}}$ of the 14 randomly constructed pairs of cluster samples. The pairs are arranged in increasing masses (from top left to bottom left, continuing from top right to bottom right). In each panel, the red horizontal dashed line denotes the theoretically expected bias ratio $r_{\text{b,th}}$ (in the absence of AB); the 3 numbers shown in blue are the masses of the early-analogous and late-analogous clusters (in unit of $10^{14} h^{-1} M_{\odot}$), and the probability for the pair to be drawn from the same parent population.

Λ CDM. The probability for the early- and late-forming halos to have the same large-scale bias is $p = 1.78 \times 10^{-4}$ using the mid-range clustering measurements.

As the final sanity check, we construct 14 pairs of random cluster samples that have similar distributions in halo mass and redshift as the $z_{20\text{ex},\text{Mz}}$ set, but chosen from the parent cluster sample *regardless* of their z_{20} , to demonstrate the robustness of our method. The random samples are generated in the following way. We first make grids in the $M-z$ space limited to that spanned by the $z_{20\text{ex},\text{Mz}}$ set, that is, $\log M_{200\text{m}}/(h^{-1} M_{\odot}) = 14 - 14.5$ and $z = 0.06 - 0.12$. To generate a random sample analogous to the early-forming clusters of the $z_{20\text{ex},\text{Mz}}$ set, we only select clusters from grids in which the number of clusters from the full sample (of 634 clusters) is at least more than two larger than the number of early-forming clusters from the $z_{20\text{ex},\text{Mz}}$ set. A late-forming cluster sample analog is generated in a similar fashion. Note that the early-analog and late-analog samples are generated independently of each other.

In Figure 3 we show the ratio $w_{p,\text{early}}/w_{p,\text{late}} = b_{\text{early}}/b_{\text{late}}$ of the 14 randomly constructed pairs of cluster samples. Each pair consists of 138 early-analog and 121

late-analog clusters, identical to that of the $z_{20\text{ex},Mz}$ set. In the upper left part of each panel, we show the masses of the early-analogous and late-analogous clusters (in unit of $10^{14}h^{-1}M_{\odot}$), and the probability for the pair to be drawn from the same parent population (using the clustering measurements within the mid-range). The red horizontal line denotes the bias ratio expected (in the absence of AB) given the masses of the cluster samples in consideration. As we arrange the pairs in increasing masses, the red line is always very close to unity (shown as the black horizontal dotted line). None of these shows probabilities as low as that of the $z_{20\text{ex},Mz}$ set.

4. SUMMARY AND PROSPECTS

Using a novel approach of combining a constrained simulation of the local universe *Elucid* with a sample of galaxy clusters from SDSS, we have constructed a pair of early- and late-forming cluster samples. The formation time indicator z_{20} of the clusters is derived from their counterpart massive halos found in *Elucid*. While WL-based cluster mass estimates indicate the two samples are comparable (within 1σ), their large-scale biases differ at such a degree that the probability for the two to be drawn from the same population is at the level of 10^{-10} , which strongly hints at a detection of AB (at $> 6\sigma$, with the correct sign that older clusters are *less* biased than the younger ones). Furthermore, the properties of the galaxy populations of the two samples are also consistent with the expectation of the age difference: the overall galaxy surface density profile is more concentrated in the early-forming clusters than that in the late-forming ones. The signal is found to be consistent with the theoretical prediction of Λ CDM. We note that in the unfortunately and unlikely ($\sim 3\%$ chance) case where the differences in clustering measurements are mainly due to the cluster mass difference, our cluster samples still exhibit an AB signal at about 4σ level.

Forward-modeling techniques like the one used to construct *Elucid*, as well as BORG (Jasche & Wandelt 2013), COSMIC BIRTH (Kitaura et al. 2021), are gaining increasing popularity, and they have immense potential for advancing our understanding of structure formation. In this study we focus on the AB related to the halo formation time. With *Elucid*, in principle we can further study AB manifested in other halo properties such as spin or concentration. Furthermore, Yang et al. (2018) have also used *Elucid* to develop the “neighborhood abundance matching”

method. Finally, with rich spectroscopic data coming from surveys like Dark Energy Spectroscopic Instrument (DESI; DESI Collaboration et al. 2016) and Subaru Prime Focus Spectrograph (PFS; Takada et al. 2014), one can expect the reconstruction to become much more reliable, particularly at higher redshifts, which would facilitate studies of AB in the distant universe.

ACKNOWLEDGMENTS

We are grateful to Rachel Mandelbaum for providing the SDSS shape catalog used in this work. We thank Yen-Chi Chen, Benedikt Diemer, Olivier Doré, Andrey Kravtsov, Neal Dalal, and You-Hua Chu for helpful comments, and Yangyao Chen for help with the *Elucid* simulation data. YTL is supported by the Ministry of Science and Technology of Taiwan under grants MOST 110-2112-M-001-004 and MOST 109-2112-M-001-005, and a Career Development Award from Academia Sinica (AS-CDA-106-M01). HM is supported by World Premier International Research Center Initiative (WPI Initiative), MEXT, Japan, and JSPS KAKENHI Grant Numbers JP20H01932 and JP21H05456. HG is supported by NSFC (Nos. 11922305, 11833005). HYW is supported by NSFC 11733004. YTL thanks IH, LYL and ALL for constant encouragement and inspiration.

Funding for the SDSS and SDSS-II has been provided by the Alfred P. Sloan Foundation, the Participating Institutions, the National Science Foundation, the U.S. Department of Energy, the National Aeronautics and Space Administration, the Japanese Monbukagakusho, the Max Planck Society, and the Higher Education Funding Council for England. The SDSS Web Site is <http://www.sdss.org/>.

The SDSS is managed by the Astrophysical Research Consortium for the Participating Institutions. The Participating Institutions are the American Museum of Natural History, Astrophysical Institute Potsdam, University of Basel, University of Cambridge, Case Western Reserve University, University of Chicago, Drexel University, Fermilab, the Institute for Advanced Study, the Japan Participation Group, Johns Hopkins University, the Joint Institute for Nuclear Astrophysics, the Kavli Institute for Particle Astrophysics and Cosmology, the Korean Scientist Group, the Chinese Academy of Sciences (LAMOST), Los Alamos National Laboratory, the Max-Planck-Institute for Astronomy (MPIA), the Max-Planck-Institute for Astrophysics (MPA), New Mexico State University, Ohio State University, University of Pittsburgh, University of Portsmouth, Princeton University, the United States Naval Observatory, and the University of Washington.

REFERENCES

- Abazajian, K. N., Adelman-McCarthy, J. K., Agüeros, M. A., et al. 2009, *ApJS*, 182, 543, doi: [10.1088/0067-0049/182/2/543](https://doi.org/10.1088/0067-0049/182/2/543)
- Chang, Y.-Y., van der Wel, A., da Cunha, E., & Rix, H.-W. 2015, *ApJS*, 219, 8, doi: [10.1088/0067-0049/219/1/8](https://doi.org/10.1088/0067-0049/219/1/8)

- Chue, C. Y. R., Dalal, N., & White, M. 2018, JCAP, 2018, 012, doi: [10.1088/1475-7516/2018/10/012](https://doi.org/10.1088/1475-7516/2018/10/012)
- Cid Fernandes, R., Pérez, E., García Benito, R., et al. 2013, A&A, 557, A86, doi: [10.1051/0004-6361/201220616](https://doi.org/10.1051/0004-6361/201220616)
- DESI Collaboration, Aghamousa, A., Aguilar, J., et al. 2016, arXiv e-prints, arXiv:1611.00036. <https://arxiv.org/abs/1611.00036>
- Feldmann, R., Carollo, C. M., Porciani, C., et al. 2006, MNRAS, 372, 565, doi: [10.1111/j.1365-2966.2006.10930.x](https://doi.org/10.1111/j.1365-2966.2006.10930.x)
- Gao, L., Springel, V., & White, S. D. M. 2005, MNRAS, 363, L66, doi: [10.1111/j.1745-3933.2005.00084.x](https://doi.org/10.1111/j.1745-3933.2005.00084.x)
- Guo, H., Li, C., Zheng, Z., et al. 2017, ApJ, 846, 61, doi: [10.3847/1538-4357/aa85e7](https://doi.org/10.3847/1538-4357/aa85e7)
- Hirata, C., & Seljak, U. 2003, MNRAS, 343, 459, doi: [10.1046/j.1365-8711.2003.06683.x](https://doi.org/10.1046/j.1365-8711.2003.06683.x)
- Jasche, J., & Wandelt, B. D. 2013, MNRAS, 432, 894, doi: [10.1093/mnras/stt449](https://doi.org/10.1093/mnras/stt449)
- Jing, Y. P., Suto, Y., & Mo, H. J. 2007, ApJ, 657, 664, doi: [10.1086/511130](https://doi.org/10.1086/511130)
- Kitaura, F.-S., Ata, M., Rodríguez-Torres, S. A., et al. 2021, MNRAS, 502, 3456, doi: [10.1093/mnras/staa3774](https://doi.org/10.1093/mnras/staa3774)
- Komatsu, E., Dunkley, J., Nolta, M. R., et al. 2009, ApJS, 180, 330, doi: [10.1088/0067-0049/180/2/330](https://doi.org/10.1088/0067-0049/180/2/330)
- Lan, T.-W., Ménard, B., & Mo, H. 2016, MNRAS, 459, 3998, doi: [10.1093/mnras/stw898](https://doi.org/10.1093/mnras/stw898)
- Landy, S. D., & Szalay, A. S. 1993, ApJ, 412, 64, doi: [10.1086/172900](https://doi.org/10.1086/172900)
- Lin, Y.-T., Mandelbaum, R., Huang, Y.-H., et al. 2016, ApJ, 819, 119, doi: [10.3847/0004-637X/819/2/119](https://doi.org/10.3847/0004-637X/819/2/119)
- Mandelbaum, R., Hirata, C. M., Leauthaud, A., Massey, R. J., & Rhodes, J. 2012, MNRAS, 420, 1518, doi: [10.1111/j.1365-2966.2011.20138.x](https://doi.org/10.1111/j.1365-2966.2011.20138.x)
- Mandelbaum, R., Slosar, A., Baldauf, T., et al. 2013, MNRAS, 432, 1544, doi: [10.1093/mnras/stt572](https://doi.org/10.1093/mnras/stt572)
- Mandelbaum, R., Hirata, C. M., Seljak, U., et al. 2005, MNRAS, 361, 1287, doi: [10.1111/j.1365-2966.2005.09282.x](https://doi.org/10.1111/j.1365-2966.2005.09282.x)
- Mansfield, P., & Kravtsov, A. V. 2020, MNRAS, 493, 4763, doi: [10.1093/mnras/staa430](https://doi.org/10.1093/mnras/staa430)
- Mao, Y.-Y., Zentner, A. R., & Wechsler, R. H. 2018, MNRAS, 474, 5143, doi: [10.1093/mnras/stx3111](https://doi.org/10.1093/mnras/stx3111)
- Medezinski, E., McDonald, M., More, S., et al. 2019, ApJ, 882, 166, doi: [10.3847/1538-4357/ab2da2](https://doi.org/10.3847/1538-4357/ab2da2)
- Miyatake, H., More, S., Takada, M., et al. 2016, Physical Review Letters, 116, 041301, doi: [10.1103/PhysRevLett.116.041301](https://doi.org/10.1103/PhysRevLett.116.041301)
- Nakajima, R., Mandelbaum, R., Seljak, U., et al. 2012, MNRAS, 420, 3240, doi: [10.1111/j.1365-2966.2011.20249.x](https://doi.org/10.1111/j.1365-2966.2011.20249.x)
- Navarro, J. F., Frenk, C. S., & White, S. D. M. 1997, ApJ, 490, 493, doi: [10.1086/304888](https://doi.org/10.1086/304888)
- Oke, J. B., & Gunn, J. E. 1983, ApJ, 266, 713, doi: [10.1086/160817](https://doi.org/10.1086/160817)
- Ostriker, J. P., & Tremaine, S. D. 1975, ApJL, 202, L113
- Reyes, R., Mandelbaum, R., Gunn, J. E., et al. 2012, MNRAS, 425, 2610, doi: [10.1111/j.1365-2966.2012.21472.x](https://doi.org/10.1111/j.1365-2966.2012.21472.x)
- Rykoff, E. S., Rozo, E., Busha, M. T., et al. 2014, ApJ, 785, 104, doi: [10.1088/0004-637X/785/2/104](https://doi.org/10.1088/0004-637X/785/2/104)
- Springel, V., White, S. D. M., Jenkins, A., et al. 2005, Nature, 435, 629, doi: [10.1038/nature03597](https://doi.org/10.1038/nature03597)
- Strauss, M. A., Weinberg, D. H., Lupton, R. H., et al. 2002, AJ, 124, 1810, doi: [10.1086/342343](https://doi.org/10.1086/342343)
- Sunayama, T., & More, S. 2019, MNRAS, 490, 4945, doi: [10.1093/mnras/stz2832](https://doi.org/10.1093/mnras/stz2832)
- Takada, M., & Jain, B. 2003a, MNRAS, 340, 580, doi: [10.1046/j.1365-8711.2003.06321.x](https://doi.org/10.1046/j.1365-8711.2003.06321.x)
- . 2003b, MNRAS, 344, 857, doi: [10.1046/j.1365-8711.2003.06868.x](https://doi.org/10.1046/j.1365-8711.2003.06868.x)
- Takada, M., Ellis, R. S., Chiba, M., et al. 2014, PASJ, 66, R1, doi: [10.1093/pasj/pst019](https://doi.org/10.1093/pasj/pst019)
- Tinker, J. L., Robertson, B. E., Kravtsov, A. V., et al. 2010, ApJ, 724, 878, doi: [10.1088/0004-637X/724/2/878](https://doi.org/10.1088/0004-637X/724/2/878)
- Tremaine, S. D., & Richstone, D. O. 1977, ApJ, 212, 311
- Wang, H., Mo, H. J., Yang, X., Jing, Y. P., & Lin, W. P. 2014, ApJ, 794, 94, doi: [10.1088/0004-637X/794/1/94](https://doi.org/10.1088/0004-637X/794/1/94)
- Wang, H., Mo, H. J., Yang, X., et al. 2016, ApJ, 831, 164, doi: [10.3847/0004-637X/831/2/164](https://doi.org/10.3847/0004-637X/831/2/164)
- Wechsler, R. H., & Tinker, J. L. 2018, ARA&A, 56, 435, doi: [10.1146/annurev-astro-081817-051756](https://doi.org/10.1146/annurev-astro-081817-051756)
- Wechsler, R. H., Zentner, A. R., Bullock, J. S., Kravtsov, A. V., & Allgood, B. 2006, ApJ, 652, 71, doi: [10.1086/507120](https://doi.org/10.1086/507120)
- Yang, X., Mo, H. J., van den Bosch, F. C., et al. 2007, ApJ, 671, 153, doi: [10.1086/522027](https://doi.org/10.1086/522027)
- Yang, X., Zhang, Y., Wang, H., et al. 2018, ApJ, 860, 30, doi: [10.3847/1538-4357/aac2ce](https://doi.org/10.3847/1538-4357/aac2ce)
- York, D. G., Adelman, J., Anderson, Jr., J. E., et al. 2000, AJ, 120, 1579, doi: [10.1086/301513](https://doi.org/10.1086/301513)
- Zu, Y., Mandelbaum, R., Simet, M., Rozo, E., & Rykoff, E. S. 2017, MNRAS, 470, 551, doi: [10.1093/mnras/stx1264](https://doi.org/10.1093/mnras/stx1264)
- Zu, Y., Shan, H., Zhang, J., et al. 2021, MNRAS, 505, 5117, doi: [10.1093/mnras/stab1712](https://doi.org/10.1093/mnras/stab1712)